Design of Probabilistically-Robust Wide-Area Power System Stabilizers to Suppress Inter-Area Oscillations of Wind Integrated Power Systems

Deping Ke, and C. Y. Chung, *Fellow, IEEE*

Abstract**--This paper proposes a systematic approach to coordinately design probabilistically-robust wide-area power system stabilizers (WPSSs) for suppressing inter-area oscillations of power systems incorporating wind power. Specifically, the operating point of the system varies stochastically due to wind power integration and each operating point corresponds to a wind power generation scenario in the steady state. Thus, the WPSSs tuned by solving a delicately formulated optimization problem can maximize the occurrence probability of scenarios where the inter-area modes possess the acceptable damping ratios, and strictly constrain their unfavorable impacts. Multiple contingencies are also directly considered. In addition, several advanced techniques are tactfully employed for accurate and efficient evaluation of occurrence probability (objective function) during the optimization so as to ensure the proposed tuning method can deal with the highly nonlinear relationships between the system eigenvalues and the steady-state power outputs of wind farms; a customized differential evolution algorithm is proposed as well to efficiently solve the formulated optimization problem. Simulations and comparisons conducted on two classic test systems with proper modifications show the effectiveness and efficiency of the proposed control design method.**

Index Terms**—Damping control, probability, inter-area oscillation, wide-area power system stabilizer, wind power.**

I. INTRODUCTION

WIND power penetration has continuously increased in many power systems, leading to more stochastic dynamics of inter-area power oscillations [1]. It has been well recognized that controllers designed by the conventional deterministic methods may perform unsatisfactorily in suppressing the inter-area oscillations in the stochastic environment [2]; new design methodologies directly taking into account the randomness of the wind power are desired.

Proposals of driving doubly fed induction generator (DFIG) based wind turbines (WTs) to assist damping of electromechanical oscillations of power systems have emerged in an increasing number of academic studies [3]-[14]. Generally, the DFIG takes part in the damping control by supplementary modulation of its (active and/or reactive) power output. Various control design techniques have been employed to verify the significant capability of the DFIG in improving damping of modes of interest, such as the heuristic tuning [4], the phase compensation technique [5], the frequency response method [6], [7], the optimal control [8], the closed-loop eigenvalue placement based optimization [9], [10] and others [11]-[14]. Driving variable-speed wind generators to contribute to frequency regulation and oscillation damping has been successfully simulated in a real power system in [15], which is a meaningful step towards applications of such studies in practice. Moreover, flexible AC transmission system (FACTS) devices which have same fast response characteristics as variable-speed wind generators can cooperate with them to improve the system dynamics, e.g. subsynchronous resonance (SSR) issue [16]. Literature [17] has developed a hierarchical scheme to coordinate FACTS devices and wind generators for short-term frequency regulation and inter-area oscillation damping. Moreover, specific issues such as the impacts of WTs' layout in wind farm (WF) on the control performance and the disaggregation of the controller synthesized based upon a single aggregated WT to multiple actual WTs are also investigated [18], [19]. However, these researchers have generally ignored the strong stochasticity caused by wind power integration. Indeed, the operating point of a power system incorporating considerable wind power randomly varies over a large range and the probability distributions of critical modes in the complex plane are necessarily employed to evaluate the small-signal stability of the system [20].

So far, a limited number of studies have proposed designs of damping controllers with direct consideration of the stochastic nature of wind power [21]-[24]. In order to gain the robustness with respect to variation of wind power generation (WPG), the damping controllers in [22] are tuned in multiple operating points created by simultaneously and uniformly increasing the steady-state power outputs of synchronous units. Furthermore, the more appropriate manner to address the randomness of wind power output is proposed in [23] where the probability distributions of the modes of interest are computed according to the probability density functions (PDFs) of the WPG, to evaluate the objective function during the process of optimizing damping controllers' parameters. Specifically, the relationships between each eigenvalue and the power outputs of all WFs are assumed to be linear for efficient probability calculations. Nevertheless, such a relationship in reality greatly depends on the dispatching strategy of the synchronous units to compensate the steady state generation-load imbalance caused by the WPG; it can be highly nonlinear. Thus, the approximated probability calculation may be inaccurate. Indeed, this issue is particularly emphasized in [24] so that the full nonlinear relationship is utilized to accurately derive the open-loop eigenvalues' probability distributions (by the probabilistic collocation method) used for the selection of a nominal operating point to synthesize

This work was supported by the Natural Science Foundation of China (Grant No.: 51307124).

D. P. Ke is with the School of Electrical Engineering, Wuhan University, Wuhan 430072, China (kedeping@whu.edu.cn).

C. Y. Chung is with the Department of Electrical and Computer Engineering, University of Saskatchewan, Saskatoon, Canada (c.y.chung@usask.ca).

the controllers. Although favorable control effects are observed, there is still much space to improve the overall damping of the system since the control design based on a selected (nominal) operating point cannot fully take into account the system's dynamic characteristics over the vast operating conditions.

In this paper, a novel systematic approach is proposed for coordinated tuning of conventionally-structured wide-area power system stabilizers (WPSSs) with probabilistic robustness to damp the inter-area oscillations of power systems incorporating wind power. Normally, the operating point of the system is stochastic due to the wind power, and each WPG scenario determines an operating point. Hence, probabilistic robustness here means that the WPSSs with optimal parameters obtained via solving a delicately proposed optimization problem can maximize the occurrence probability of the scenarios in which the closed-loop system has required damping ratios for all the inter-area modes, and also strictly constrain their adverse impacts over all the scenarios. Furthermore, such robustness requirement is not only for the system which is in the normal condition, but also meaningfully for the post-contingency system which is normally quite vulnerable. Specifically, the occurrence probability is approximated during the optimization by employing the advanced scenario generation and model reduction techniques so that the calculation can be quite efficient and accurate even when the relationships between the system eigenvalues and the steady-state power outputs of WFs are highly nonlinear. Moreover, together with a proposed customized differential evolution (DE) algorithm to solve the optimization, the proposed tuning method has quite a favorable computational efficiency to obtain the optimal WPSSs which can perform as expected to damp the inter-area oscillations.

The remainder of this paper is organized as follows. Section II introduces WPSSs to damp inter-area oscillations of power systems with uncertain WPG. Section III formulates the optimization for tuning the WPSSs' parameters. Section IV introduces the relevant techniques to lower the computational intensity of the probability calculations during the optimization. Section V presents the customized DE. Simulation results and analysis are shown in Section VI. Section VII concludes the paper.

II. Employment of WPSSs to Suppress Inter-Area Oscillations in Power Systems with Wind Power

Suppose there are N_w WFs connected to a power system. The steady-state active power outputs (p_{w1}, p_{w2}, $\cdots$, p_{wN_w}) of the WFs are stochastic because of the uncertain wind speed. Specifically, a WPG scenario represents a case of concurrent power outputs of the WFs in the steady state. For example, the ith scenario $S^{(i)}$ is in the following form:

$$S^{(i)} = \left[p_{w1}^{(i)}, p_{w2}^{(i)}, ..., p_{wN_w}^{(i)} \right] \tag{1}$$

Hence, a set of WPG scenarios ($S^{(1)}$, $S^{(2)}$, $\cdots$, $S^{(Nt)}$) are generally used to exactly characterize the joint probability distribution of the WFs' power outputs (N_t is the number of scenarios).

It is noted that the WFs and traditional synchronous generators together supply the system's loads. Thus, in order to keep the overall generation-load balance of the system in the steady state, several traditional (thermal or hydro) units dispatch to compensate the power imbalance caused by uncertainties in supply of wind power. Generally, which synchronous units are selected to compensate the power imbalance and how much each of them can compensate depends upon the system dispatching strategy. Thus, in the context of the dispatching strategy, each WPG scenario determines a solution of the load flow and ultimately an operating point of the system. In other words, the dispatching strategy decides the relationships between eigenvalues of the system and the steady-state power outputs of the WFs. Indeed, due to the complexity of the dispatching strategy, the relationships can be highly nonlinear (this is the case later in Section VI-B). Furthermore, it is easy to understand the stochastic impacts of wind power on the electromechanical modes which are closely associated with the power outputs of the synchronous generators. Thus, the poorly damped inter-area modes in which many synchronous units of the system participate are specially addressed in this paper and the stochasticity induced by integration of wind power is fully considered in the design of WPSSs to effectively damp them.

The above discussion concerns the WPSSs design which does not consider any component loss of the power system (in other words, it is termed that the power system is in the normal condition). Indeed, the inter-area oscillations problem usually becomes more serious when the power system loses some of its components, e.g. generator/line outages (the power system is in the emergent conditions). Therefore, the design of WPSSs in this paper also takes into account these emergent conditions. It should be noted that the control design here is just based on the linearization around the steady-state operating point of the emergent (normal) condition. Moreover, only "N-1" contingencies are considered in this study. In particular, each WPSS which is deployed in the decentralized manner employs the conventional phase lead-lag structure (Fig. 1) and its parameters (gain K and time constants T) can be adjusted to fulfill the required control objectives. Additionally, it is assumed that the dedicated communication channel is utilized to deliver remote signals to the WPSSs for enhancement of effectiveness in damping the inter-area modes; the time-delays (with the exponential forms in the Laplace domain) associated with the signal transmission is rationalized and approximated by a second-order Pade formula. Consequently, according to the procedure given in Appendix, the state matrix of the closed-loop system can be synthesized as follows [25]:

$$A^{(i,m)} = \begin{bmatrix} A_o^{(i,m)} + B_o^{(i,m)} D_c D_\tau C_o^{(i,m)} & B_o^{(i,m)} D_c C_\tau & B_o^{(i,m)} C_c \\ B_\tau C_o^{(i,m)} & A_\tau & \mathbf{0} \\ B_c D_\tau C_o^{(i,m)} & B_c C_\tau & A_c \end{bmatrix} \tag{2}$$

Here, A, B, C and D represent the state matrix, the input matrix, the output matrix and the feedforward matrix, respectively; subscripts o, τ and c indicate that the relevant matrices are derived from the linearized open-loop power system model, the approximated time-delay, and the WPSSs, respectively; superscript '(i, m)' means that the matrix is calculated based on linearization around the operating point determined by the ith WPG scenario and the mth emergent condition (m=0 denotes the normal condition). Thus, to compute the eigenvalues of $A^{(i,m)}$ over all the WPG scenarios in the *m*th emergent condition by using Monte-Carlo Simulation (MCS), probability distributions of eigenvalues in the complex plane can be obtained for evaluation of the WPSSs' performance in this emergent condition with the stochastic WPG. In other words, tuning the WPSSs should be towards the objectives defined, based on the probability distributions of the eigenvalues. This will be presented in detail in the following section.

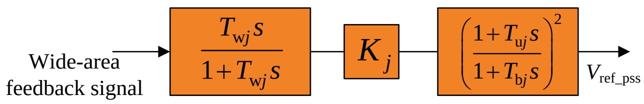

Fig. 1. Structure of WPSS (subscript *j* denotes the *j*th WPSS)

III. Formulation of An Novel Optimization Problem to Tune WPSSs

Based on the aforementioned notion that probability distributions of eigenvalues in the complex plane can be employed to evaluate the WPSSs' performance, a novel optimization problem formulated to adjust the WPSSs' parameters so as to acquire reasonable damping control effects in the stochastic environment is proposed in this section. Therefore, the objective of tuning the WPSSs is firstly addressed; then, the constraints imposed on the tuning process are introduced. Accordingly, the optimization problem which is a mathematical form to represent the objective and constraints is subsequently constructed to search the optimal parameters of the WPSSs.

A. Objective of Adjusting WPSSs' Parameters

In the normal condition or any emergent condition, the operating point of the system varies over quite a large range due to the uncertainty of wind power. Moreover, several constraints (addressed later) are imposed on the tuning process of the WPSSs. Therefore, it may be impossible for the WPSSs to enhance the damping ratios of all the inter-area modes to the required levels in all the WPG scenarios. Under such circumstance, the index to indicate the performance of the WPSSs is formed as follows:

$$Prob^{(m)} = Pr\left(\xi_1^{(m)} \geq \bar{\xi}_1^{(m)},\ \xi_2^{(m)} \geq \bar{\xi}_2^{(m)}, \dots, \xi_{N_a^{(m)}}^{(m)} \geq \bar{\xi}_{N_a^{(m)}}^{(m)}\right) \quad (3)$$

where $N_a^{(m)}$ is the number of the targeted inter-area modes that are poorly damped in the *m*th emergent condition, and they are successively numbered from 1 to $N_a^{(m)}$; $Pr(\cdot)$ is the operator for calculating the occurrence probability of the (joint) incident within the parentheses; ξ is the damping ratio defined as

$$\xi = -\alpha \Big/ \sqrt{\alpha^2 + \omega^2} \quad (4)$$

with α and ω denoting the real and imaginary parts of the eigenvalue, respectively; $\bar{\xi}_1^{(m)}$, $\bar{\xi}_2^{(m)}$, $\cdots$, $\bar{\xi}_{N_a^{(m)}}^{(m)}$ are the specified positive numbers representing the acceptable damping ratios of the inter-area modes. Apparently, the index $Prob^{(m)}$ measures the occurrence probability of the joint incident that all inter-area modes in the *m*th emergent condition have acceptable damping ratios simultaneously. Specifically, use of the joint incident to build the index is innovative yet actually feasible because in any WPG scenario the WPSSs is regarded to have the required performance only when the inter-area modes concurrently have the required damping ratios.

According to the above discussion, it is easy to infer that the finely tuned WPSSs should be able to increase the index $Prob^{(m)}$ in the normal condition and all emergent conditions as much as possible. So, this is also the general guidance to build the objective function in the later subsection.

B. Constraints on Tuning Process of WPSSs

Although the proposed control design aims to augment the proportion of the scenarios in which all inter-area modes simultaneously have acceptable damping ratios, the damping controllers should not alter their frequencies too much in any possible scenario because large frequency excursions implying great changes in synchronizing torques of the synchronous generators can unfavorably influence the transient stability of the system [25]. Specifically, the index named frequency drift ratio to gauge the impacts of the WPSSs on the frequency of an eigenvalue is defined in this study, as follows:

$$\left|\Delta\omega\right|\% = \left|\omega - \omega_o\right| / \omega_o \quad (5)$$

where ω_o stands for the frequency of the eigenvalue in the open-loop state.

Besides the constraints on the frequency drift ratios of the targeted inter-area modes, it is in general required that the WPSSs cause strictly limited adverse impacts on the other eigenvalues in terms of their damping ratios and frequency drift ratios in any WPG scenario. Therefore, the next subsection will mathematically translate these constraints into the optimization problem.

C. Optimization Problem to Tune WPSS

The previous two subsections have addressed the objective and constraints for tuning of the parameters of the WPSS to achieve feasible control effects. Hence, in this subsection they are converted to the mathematical forms—the optimization problem whose solution represents the optimal parameters of the WPSSs, as follows:

$$\max_{\boldsymbol{X}} \sum_{m=0}^{N_{con}} W^{(m)} Prob^{(m)} \quad (6)$$

$$\text{s.t.} \quad Pr\left(\left|\Delta\omega_j^{(m)}\right|\% \leq WC_j^{(m)}\right) = 1 \quad j = 1, 2, \dots, N_a^{(m)}$$
$$m = 0, 1, 2, \dots, N_{con} \quad (7)$$

$$Pr\left(\left|\Delta\omega_s^{(m)}\right|\% \leq WC_s^{(m)}\right) = 1 \quad \text{for all } s \in \Omega_\omega^{(m)} \quad (8)$$

$$Pr\left(\xi_t^{(m)} \geq \bar{\xi}_t^{(m)}\right) = 1 \quad \text{for all } t \in \Omega_\alpha^{(m)} \quad (9)$$

$$\mathbf{X}^{\min} \leq \boldsymbol{X} \leq \mathbf{X}^{\max} \quad (10)$$

where symbol $\left|\Delta\omega_j^{(m)}\right|\%$ denotes the frequency drift ratio of the *j*th (inter-area) mode in the *m*th emergent condition (according to (5)), and $WC_j^{(m)}$ is the specified allowable frequency drift ratio of this mode; similar explanations can be easily inferred for symbols in (8) for the modes whose indexes are in the collection $\Omega_\omega^{(m)}$; the collection $\Omega_\alpha^{(m)}$($\Omega_\omega^{(m)}$) contains the indexes of the modes (except for the targeted inter-area modes) whose damping ratios (frequencies) can be greatly altered by the controllers in the *m*th emergent condition; $Pr(\cdot)=1$ indicates that the incident within the parentheses happens in all WPG scenarios; $\mathrm{N}_{\mathrm{con}}$ is the number of the emergent conditions; $W^{(m)}$ is the weight to indicate relative priority of optimizing the WPSSs' performance in the *m*th emergent condition; and $\boldsymbol{X}$ is the vector consisting of the adjustable parameters of the WPSSs (time constants *T* and gains *K* in Fig. 1).

There are several design parameters in the optimization such as the weights in the objective function ($W^{(0)}$, $W^{(1)}$, $W^{(2)}$, $\cdots$, $W^{(\mathrm{N}_{\mathrm{con}})}$) and the acceptable damping ratios of the inter-area modes ($\overline{\xi}_1^{(m)}$, $\overline{\xi}_2^{(m)}$, $\cdots$, $\overline{\xi}_{\mathrm{N}_\mathrm{a}^{(m)}}^{(m)}$). It is obvious that different selection of these parameters results in different control effects. Heuristically speaking, relatively larger $W^{(m)}$ will give more priority to enhance the WPSSs' performance in the *m*th emergent condition. Thus, it is suggested that $W^{(0)}$ (corresponding to the normal condition) could be much larger than the rest of the weights because power systems have much more time to operate in the normal condition than the emergent conditions. Furthermore, the damping ratio (ξ) represents the decay rate of the oscillation amplitude: it costs about $1/(2\pi\xi)$ of the oscillation period to decay to 37% of its initial value [26]. Therefore, the acceptable damping ratios can be selected according to the periods of the oscillations so that the oscillations can be damped within a desirable time. The residue analysis can be employed to initially identify the eigenvalues in $\Omega_\alpha^{(m)}$ and $\Omega_\omega^{(m)}$. Moreover, if any eigenvalue remains uncollected by the sets and is seriously deteriorated after the optimization, it is added to the sets for a new round of optimization. Thus, $\overline{\xi}_t^{(m)}$ and $\mathrm{WC}_s^{(m)}$ are set according to the open-loop values of the eigenvalues contained by the sets.

The optimal parameters of the WPSSs can be obtained by solving the above optimization problem. However, evaluation of the objective function poses a great challenge to the search process. It has been specially pointed out in Section II that damping ratios of the eigenvalues are the highly nonlinear functions of the WFs' steady-state power outputs. So, the terribly low accuracy may be totally intolerable if the linear functions are used to approximate their relationships in order to perform the fast probability calculations, just as various cumulant-based methods do. When the MCS is conducted over the set of the N_t WPG scenarios (Section II), $Prob^{(m)}$ can be accurately calculated as follows:

$$Prob^{(m)} = \mathrm{N}_{\mathrm{ok}}^{(m)} / \mathrm{N}_\mathrm{t} \tag{11}$$

where $\mathrm{N}_{\mathrm{ok}}^{(m)}$ is the number of scenarios (among the N_t scenarios) in which the joint incident happens in the *m*th emergent condition. Nevertheless, it is helpless in solving the problem if N_t is quite large because repeated calculations (11) based on the MCS with such a large number of scenarios in the normal and all emergent conditions during the search process are prohibitively expensive in terms of computational time and resources. So, this paper proposes to employ some advanced techniques to remarkably reduce the computational intensity of the objective function but with little deterioration of its accuracy, and the detailed implementing procedure is given in the next section.

IV. Reduction of Computational Intensity of Objective Function

A. *Generation of Scenarios by Latin Hypercube Sampling*

According to the above analysis, a highly efficient sampling technique which can accurately characterize the joint probability distribution of the WPG by producing a small number of scenarios is needed [24], [27]. Therefore, this paper adopts the Latin Hypercube Sampling (LHS) which is readily implementable to generate the scenario set for the probability calculations. The procedure to obtain the scenarios is summarized as follows:

1) The marginal cumulative distribution function (CDF) of each WF's power output can be derived by converting the wind speed's CDF through the WF's power conversion curve, or by cumulating the WF's actual power output series recorded over a long term. Then, according to the number of the WFs and the coverage capability of the LHS [27], the number of samplings (N_t) is determined. A number series [$1/\mathrm{N}_\mathrm{t}$, $2/\mathrm{N}_\mathrm{t}$, …, $\mathrm{N}_\mathrm{t}/\mathrm{N}_\mathrm{t}$] is generated, and each element of this series denotes a cumulative probability value. Thus, with the marginal CDF of a WF, each cumulative probability value can produce a corresponding value representing power output of the WF according to the mapping operation shown in Fig. 2 (the horizontal and vertical dash lines). All N_t values ($\mathrm{p}_\mathrm{w}^{(1)}$, $\mathrm{p}_\mathrm{w}^{(2)}$, …, $\mathrm{p}_\mathrm{w}^{(\mathrm{N}_\mathrm{t})}$) derived from the mapping operation compose the power output samplings of the WF. Apparently, such LHS procedure is also applicable for the other WFs to generate their power output samplings.

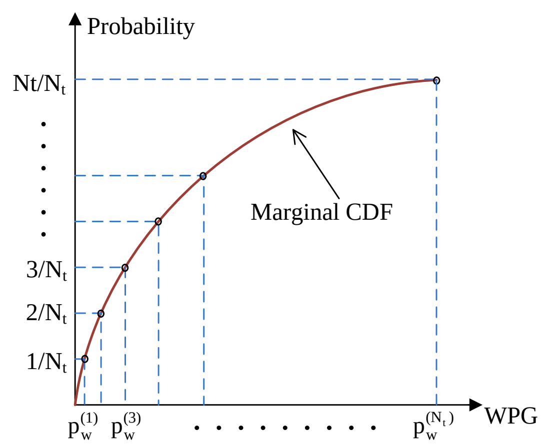

Fig. 2. Rationale demonstration of LHS

2) The coefficients of mutual correlations among all WFs' power output samplings series derived in Step 1) are either 1 or -1. So, the Cholesky decomposition based permutation is employed to rearrange the positions of the elements in these series in order to make the correlation coefficients equal to the real values among the WFs in practice. After the permutation, the WPG scenario set (with well limited number of scenarios) is obtained. Details of the Cholesky decomposition based permutation can be found in [27].

B. *Model Reduction*

In general, the dimension of the original open-loop power system model is quite high. Thus, although the number of WPG scenarios has been remarkably limited, calculating eigenvalues of the highly dimensional closed-loop state matrix $A^{(i,m)}$ for all scenarios in the normal and emergent condition is still time consuming. Because the optimization process has to repeat such calculations many times, it is necessary to reduce the dimension of the open-loop power system model (dimension of $A^{(i,m)}$ decreases correspondingly). Hence, given the original linearized model (denoted by ($A_o^{(i,m)}$, $B_o^{(i,m)}$, $C_o^{(i,m)}$)) of the open-loop power system in the *i*th WPG scenario and the *m*th emergent condition, a reduced system (described by ($A_r^{(i,m)}$, $B_r^{(i,m)}$, $C_r^{(i,m)}$)) with a much lower dimension can be acquired by using the model reduction technique. All original full open-loop system models will undergo such reduction for the control design. Consequently, as $A_r^{(i,m)}$, $B_r^{(i,m)}$, and $C_r^{(i,m)}$ are used to replace $A_o^{(i,m)}$, $B_o^{(i,m)}$, and $C_o^{(i,m)}$ in (2) for eigenvalues calculation, evaluation of the objective function by (11) can considerably reduce computational time.

Apparently, the linearization and subsequent reduction of the open-loop power system models in the normal and emergent condition over all the WPG scenarios have to consume non-ignorable time. However, thanks to the limited number of scenarios and the existing efficient model reduction methods suitable for large-scale power systems [28], this time cost is generally viable for the control design. Most important of all, preprocessing the open-loop models enables the subsequent tuning of the WPSSs' parameters; these time-consuming manipulations are excluded in the iterative search process.

According to (11), it is noted that the objective function is discretely evaluated, implying that the gradient-based optimization algorithms are ineffective to solve (6)-(10). Thus, a customized DE algorithm is proposed and introduced in the next section to deal with the optimization problem.

V. Customized DE Algorithm to Solve Formulated Optimization Problem

Depending on the characteristics of the optimization problem to be solved, a customized DE algorithm which is induced from the standard DE algorithm is proposed in this section. Firstly, before proceeding to the proposed customization, the brief procedure of the standard DE to solve the problem is introduced. Then, the low computational efficiency of the standard DE to deal with this problem is analyzed, and accordingly the characteristics of the problem are explored to customize the DE so that its efficiency can be enhanced. Finally, the customized DE is introduced in detail.

A. Standard DE to Solve the Optimization Problem

The standard DE procedure to solve the problem is described in brief as follows [29]:

1) Initialization: Define a population (parents) with N_p individuals and each individual denotes a candidate of the WPSSs' parameters vector ($\boldsymbol{X}_k$, k=1, 2,…, N_p); initialize $\boldsymbol{X}_k$ randomly within the boundaries of the parameters. A scalar fitness function $F(\cdot)$ is defined according to the objective and constraint functions to indicate the qualities of the candidates (the definition is trivial and not displayed here for brevity). Specifically, the smaller is the fitness function, better the candidate is.

2) Evaluation of parents: Calculate $F(\boldsymbol{X}_k)$ (k=1, 2,…, N_p).

3) Identify the best candidate $\boldsymbol{X}_{\text{best}}$.

4) Mutation and crossover: A new population (children) with N_p individuals ($\boldsymbol{Y}_k$, k=1, 2,…, N_p) is generated by mutation and crossover. Specifically, the DE/current-to-best/1 strategy is used for the mutation while the two-point crossover is employed [29].

5) Evaluation of children: Calculate $F(\boldsymbol{Y}_k)$ (k=1, 2,…, N_p)

6) Comparison and selection:

$$\boldsymbol{X}_k=\begin{cases}\boldsymbol{X}_k & F\left(\boldsymbol{X}_k\right)\le F\left(\boldsymbol{Y}_k\right)\\ \boldsymbol{Y}_k & F\left(\boldsymbol{X}_k\right)> F\left(\boldsymbol{Y}_k\right)\end{cases}\quad k=1, 2,\ldots, N_p \tag{12}$$

7) Termination check: If the termination condition is met or the iteration number reaches the maximum, stop calculation and treat output $\boldsymbol{X}_{\text{best}}$ as the result; otherwise, go to 3).

B. Efficiency of Standard DE and Incentives to Improve It

Generally, N_p should be large enough to ensure the global search capability of the standard DE. In each generation of the standard DE, exact evaluation of the fitness function requiring calculation of eigenvalues of $A^{(i,m)}$ over all the scenarios and the normal/emergent conditions should be repeatedly conducted, N_p times. It is readily understood that the computational time in such case will be unsatisfactory even for a small-size power system.

It is quite clear that the most computational burden of the search algorithm is the repeated eigenvalue calculations. Moreover, it is observed that exactly calculating all eigenvalues to evaluate the fitness functions in each generation is just for ordering the individuals and finally selecting the best one. In general, the ordering and selecting operations are unnecessary to exactly evaluate all candidates. For example, the classic "N-1" security scanning uses a fast preprocessor to filter out most contingencies and reserves only a small number of "potentially dangerous" contingencies for the subsequent exact but time-consuming evaluations. Thus, such idea is employed in this paper. Like the fast (linear) DC load flow is used to construct the preprocessor in the "N-1" security scanning, a fast estimation method of eigenvalues is proposed to efficiently identify a small number of individuals which would be quite possibly the best one in the generation.

With any parameters vector $\boldsymbol{X}$, the linear prediction of a closed-loop eigenvalue in the *i*th scenario and the *m*th emergent condition can be obtained as follows:

$$\bar{\lambda}^{(i,m)}=\lambda_0^{(i,m)}+\left(\partial\lambda^{(i,m)}/\partial\boldsymbol{X}\Big|_0\right)\left(\boldsymbol{X}-\boldsymbol{X}_0\right) \tag{13}$$

where $\boldsymbol{X}_0$ is the constant parameters vector; $\lambda_0^{(i,m)}$ is the value of this eigenvalue as $\boldsymbol{X}_0$ is used as the WPSSs' parameters; and $\partial\lambda^{(i,m)}/\partial\boldsymbol{X}|_0$ is the corresponding sensitivity vector evaluated at $\boldsymbol{X}_0$. Here, $\boldsymbol{X}_0$ can be obtained by using the traditional phase-compensation technique to increase the damping of the targeted inter-area modes when the system is in the nominal operating condition. If sensitivity vectors of all eigenvalues are calculated and stored in advance of the optimization, the time cost to derive the linear predictions of these eigenvalues is almost negligible compared to that required to calculate the exact values. Actually, such linear prediction of eigenvalues has been widely used in the extant literatures [1], [20].

C. Customized DE to Solve the Optimization Problem

The proposed customized DE has almost the same procedure as that of the standard DE but with the following specific changes:

C1) Evaluation of parents: The linear predictions of the eigenvalues in all scenarios are computed according to (13) with $\boldsymbol{X}_k$ (k=1, 2,…, N_p) and the stored sensitivity vectors. Then, an estimation of $F(\boldsymbol{X}_k)$ denoted by $\bar{F}(\boldsymbol{X}_k)$ is calculated by simply evaluating the fitness function with predictions of the eigenvalues, and $\boldsymbol{X}_k$ is ranked in accordance to the ascending order of $\bar{F}(\boldsymbol{X}_k)$. Thereafter, $F(\boldsymbol{X}_k)$ is computed for the first N_e(N_e<<N_p) of the ordered $\boldsymbol{X}_k$.

C2) $\boldsymbol{X}_{best}$ is identified just among the candidates whose $F(\boldsymbol{X}_k)$ have been evaluated, rather than all $\boldsymbol{X}_k$.

C3) Evaluation of children: Analogously to C1, $\bar{F}(\boldsymbol{Y}_k)$ are calculated for all children ($\boldsymbol{Y}_k$) while $F(\boldsymbol{Y}_k)$ are evaluated just for the first N_e superior children indicated by $\bar{F}(\boldsymbol{Y}_k)$.

C4) Comparison and selection: When $\boldsymbol{X}_k$ and $\boldsymbol{Y}_k$ are compared, $\boldsymbol{X}_k$ will survive in the next generation if any one of the following conditions is satisfied: (i) both $F(\boldsymbol{X}_k)$ and $F(\boldsymbol{Y}_k)$ are evaluated and $F(\boldsymbol{X}_k) \le F(\boldsymbol{Y}_k)$; (ii) only $F(\boldsymbol{X}_k)$ is evaluated; (iii) neither $F(\boldsymbol{X}_k)$ nor $F(\boldsymbol{Y}_k)$ is evaluated and $\bar{F}(\boldsymbol{X}_k) \le \bar{F}(\boldsymbol{Y}_k)$. Otherwise, $\boldsymbol{Y}_k$ will replace the position of $\boldsymbol{X}_k$ in the population (parents) of the next generation.

The customized DE exactly assesses only a small part (N_e) of the candidates in each generation; its computational efficiency is much higher than that of the standard DE. As done by the standard DE, the customized DE applies the same mutation and crossover over the N_p candidates for adequately exploring the search space. Notably, the exactly evaluated candidates in the customized DE are quite possibly the most superior ones in the population according to the ranking of the estimated fitness functions. Hence, although only a part of candidates are exactly evaluated for the competition and evolution, the customized DE will not miss the 'fine genes' derived from the genetic operations and will collect them from generation to generation as they are normally carried by the superior candidates. So, the exploitation and exploration capabilities of the customized DE ensure that its search quality is not significantly sacrificed with respect to the standard DE.

VI. Simulation Test and Analysis

In this section, two classic test systems (the four-machine two-area system and the New York and New England interconnected system) are modified and simulated to validate the proposed WPSS design. The two systems have different characteristics in terms of the size and components so as to sufficiently examine the generalized effectiveness of the proposed control design under different test environments. All simulations conducted in this section are with the open-source Matlab based software package — PSAT (Power System Analysis Toolbox) [30]. The computing platform is a desktop with Intel Dual-Core i5-2320 CPU of 3.00 GHz and 4.00GB RAM.

A. Two-Area System

1) System Description and Settings for Control Design

The first modification to the two-area system is a WF attached to Bus-6 (Fig. 3). All WTs in the WF are aggregated to a DFIG-based WT, and the installed capacity of the WF is 1200 MW. Specifically, the active load of Bus-6 is additionally increased by 600 MW. Thus, the peak penetration level of wind power in this system is up to 35%. Furthermore, another significant change to the original two-area system is a HVDC line which connects Bus-7 and -9. The control system of the HVDC line based on line-commuted converters is to ensure constant power transmission (300 MW) carried by the line. Particularly, in order to compensate reactive power consumed by the HVDC line, two additional shunt capacitors are installed at Bus-7 and -9 to provide the reactive power of 225 Mvar and 100 Mvar, respectively, in the nominal voltage level. Appendix gives the parameters of the DFIG and the HVDC line, and the data of the original two-area system can be found in [26].

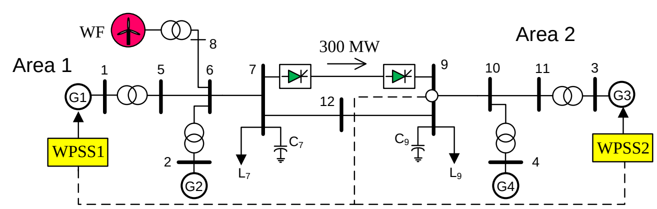

Fig. 3. Modified two-area system with a WF and a HVDC line

Weibull distribution with the shape parameter 1.6 and the scale parameter 15 is assumed for wind speed in this test. So, by using simple random sampling (SRS) technique, a number of wind speed data (N_t=10000) is generated to mimic the actual wind speed variation; then, a WPG scenario set with 10000 scenarios is obtained by converting the wind speed to the WPG, as follows:

$$p_w = 0.5\pi R^2 \rho_{air} V_w^3 C_p^{opt}\left(V_w\right) \tag{14}$$

where R is the radius of the WT blade; ρ_{air} is the air density; V_w is the wind speed; and $C_p^{opt}(\cdot)$ denotes the optimal power conversion curve of the WT with respect to the wind speed. The parameters of the WT refer to those in [31]. In the scheduled steady state, the WF's power output is assumed to be the expected value (EV) which can be calculated from the WPG scenarios. Here, the EV of the WPG is 612 MW. If the real WPG (p_w) in the steady state deviates from the EV ($\bar{p}_w$), it is proposed that their difference ($p_w - \bar{p}_w$) is equally accommodated by the synchronous generators in order to keep balance between the power generation and consumption, i.e., the real steady-state power output of each synchronous generator will be its scheduled value minus 0.25($p_w - \bar{p}_w$).

Eigen-analysis with the above dispatching strategy shows that a poorly damped inter-area mode consistently exists over all the WPG scenarios; it is obviously observed in the electromechanical power oscillation between Area 1 and 2 (G_1, G_2 vs. G_3, G_4). Moreover, each area has a well damped local mode which dominates the relative motion between the synchronous generators in the area. Besides the normal system condition (configuration) shown in Fig. 3, five more emergent conditions are also considered for this system (Table I). Here, the first four conditions are directly included during the control design while the last two are just for the control effect validation. It should be pointed out that the average WPG imbalance to be accommodated by each synchronous unit is $(p_w-\bar{p}_w)/3$ with the contingencies 1 and 2. Analogous damping situations associated with the inter-area and local modes as those in the normal condition are found in these emergent conditions. Thus, WPSSs are employed to improve the inter-area mode's distribution in the complex plane in the normal/emergent conditions.

In this paper, the bus frequency which is the derivative of bus voltage phase angle is used as feedback signals for the WPSSs. While different buses' frequencies are attempted as the feedback signals and different synchronous generators are tried as the WPSS installation site, residue analysis over a large number of WPG scenarios along with consideration of the emergent conditions indicates that G_1 and G_3 are the appropriate sites to install WPSSs and the frequency of Bus-9 is the most effective feedback signal. The time-delays of the two communication channels are commonly assumed to be 80 ms. The acceptable damping ratios in the normal/emergent conditions ($\bar{\xi}_1^{(0)}$, $\bar{\xi}_1^{(1)}$, $\bar{\xi}_1^{(2)}$, $\bar{\xi}_1^{(3)}$, $\bar{\xi}_1^{(4)}$ and $\bar{\xi}_1^{(5)}$) are set to be 0.1, 0.08, 0.08, 0.1, 0.08 and 0.08 respectively; and the allowable frequency drift ratios ($\mathrm{WC}_1^{(0)}$, $\mathrm{WC}_1^{(1)}$, $\mathrm{WC}_1^{(2)}$, $\mathrm{WC}_1^{(3)}$, $\mathrm{WC}_1^{(4)}$ and $\mathrm{WC}_1^{(5)}$) are uniformly selected to be 0.15. For the control design, the LHS generates 200 WPG scenarios (N_t=200) which have the marginal CDF of the WF's power output very close to that in the actual WPG scenarios (N_t=10000). Then, the Schur balanced truncation method is employed to conduct the model reductions over all the reduced WPG scenarios in the normal/emergent conditions. For the sake of implementation simplicity, the orders of all reduced models are uniformly chosen to be 12. The weights ($W^{(0)}$, $W^{(1)}$, $W^{(2)}$ and $W^{(3)}$) are set to be 1.0, 0.5, 0.5 and 0.5, respectively. The optimization parameters N_p and N_e are set to be 60 and 5, respectively.

TABLE I
INDEX *prob*$^{(m)}$ IN NORMAL/EMERGENT CONDITIONS OF TWO-AREA SYSTEM

No.	Contingency	Exact	Appr.	Robust
0	Nominal	0.9142	0.9250	0.8503
1	G_1 outage	0.6633	0.6950	0.4428
2	G_3 outage	0.5965	0.6200	0.4057
3	HVDC line outage	0.8801	0.8650	0.7996
4	G_2 outage	0.7479	0.7450	0.5312
5	G_4 outage	0.7531	0.7750	0.6485

2) Search Efficiency and Capability of Customized DE

In order to relieve the tremendous computational burden during the optimization, it consumes about 80 s to conduct the model reductions in the normal and emergent conditions with all the reduced WPG scenarios. After that, the proposed customized DE is compared with the standard DE in terms of their search efficiencies and capabilities, via dealing with the same optimization. Firstly, the customized DE is run 30 times to solve the optimization problem; likewise, the standard DE computes the optimization, 5 times. Hence, statistical results show that the average time cost to complete the computations of one generation by the customized DE is 1.83 s (this time consumption is about 115 s if neither model reduction nor WPG scenario reduction is conducted). Moreover, evolutions of the objective function during the search of these two algorithms are depicted in Fig. 4. It is clear that the average convergence characteristic of the customized DE (it takes about 575 generations to converge on average) is never inferior to that of the standard DE. Meanwhile, 90% of the search runs by the customized DE converge to almost same maximum value which is also the best result obtained by the standard DE.

Based on the above comparisons, it is easily concluded that the customized DE is appropriate and effective to cope with the optimization used for tuning of the WPSSs. Its computational efficiency is favorable and much higher than that of the standard DE.

3) Control Effects of Derived Optimal WPSSs

The optimal WPSSs' parameters which are corresponding to the maximum objective function value derived in the previous part are listed in Appendix. So, the index *prob*$^{(m)}$ is computed based on these optimal parameters for each normal/emergent condition. When the real WPG scenarios (N_t=10000) and the full linearized models are employed, the derived value of *prob*$^{(m)}$ can be used as the benchmark for the (approximate) calculation result which uses the reduced WPG scenarios (N_t=200) and the reduced models (Table I). It is readily seen that the approximate *prob*$^{(m)}$ is very close to its real value (benchmark) in all the normal and emergent conditions, which indicates that the proposed countermeasures to low the computational burden are feasible and the obtained optimization result is receivable.

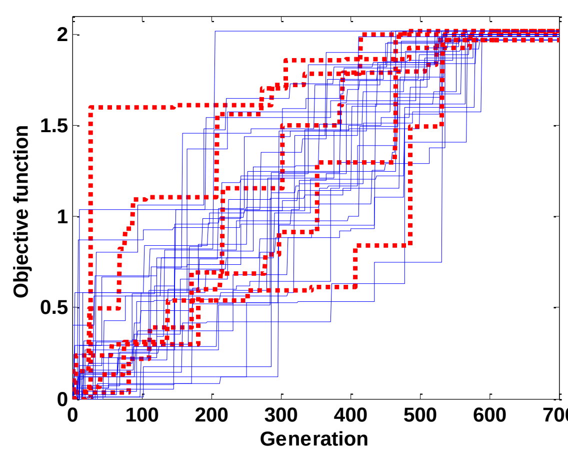

Fig. 4. Search process of DE (dot line: standard; solid line: customized)

According to Table I, the inter-area mode in the normal condition being subject to the stochastic WPG has the largest probability to obtain the acceptable damping ratio. This is because the tuning process of the WPSSs gives more priority to enhance their performance in the normal condition ($W^{(0)}$ is obviously larger than the other weights). Moreover, since there is only one WPSS operating in the emergent conditions 1 and 2, it is not surprised to see that the inter-area mode has relatively lower probability to locate in the desirable region of the complex plane in these two conditions. An interesting phenomenon is that although the DC line is outage in the emergent condition 3, the WPSSs' performance is not significantly influenced, compared to that in the normal condition. Furthermore, the index $Prob^{(m)}$ is also calculated for the emergent conditions 4 and 5 which are not directly involved in the design. No serious degeneration of this index is observed in these two conditions in contrast to that in the normal condition (in fact, the two index values are better than those in the emergent conditions 1 and 2).

In order to highlight the proposed probabilistic design of the WPSSs, a robust design, akin to the one used in [24] is employed for the comparison. Specifically, the design employs the linearized open-loop system model derived as the system is in the normal condition and the WF's power output is the EV. With the WPSSs tuned by this method, the index $Prob^{(m)}$ is computed and also shown in Table I. Clearly, the proposed probabilistic design is entirely superior to the robust design, especially for the emergent conditions. Additionally, Fig. 5 delineating the distribution of the inter-area mode in the complex plane in the emergent condition 5 is a direct visual evidence of this conclusion. Particularly, in this figure the points lying outside the desirable region are related to the scenarios in which the WF's power outputs are much less than the EV. This can be heuristically explained by the fact that the insufficient power supply by the WF will be compensated by the synchronous units (outputting more power), which tends to impair the damping of the inter-area mode. Actually, similar phenomenon is also observed in the normal and other emergent conditions.

Time-domain simulations are carried out to verify the performance of the WPSSs when the system is in different operating points. For example, as the system is in the normal condition and the WF outputs the expected power, an instantaneous three-phase short-circuit fault which occurs at Bus 12 and lasts for 50 ms evokes the system dynamics shown in Fig. 6. Obviously, the WPSSs effectively behave to damp the inter-area oscillation. Moreover, the terminal voltage of G_1 and G_3 is not considerably impacted by the WPSSs and has the favorable profiles due to the proper constraints on the WPSSs' gains during the design stage and also the hard limiters on the WPSSs' outputs. Another example is obtained when the system is in the emergent condition 5 and the WF outputs the power of 100 MW so that in the steady state the direction of the power flow carried by the AC line 7-12 is from Area 2 to 1 (in most of the scenarios the direction is from Area 1 to 2). Then, the same fault as that in the previous example is applied and Fig. 7 collects the system dynamics. Comparatively speaking, the WPSSs' performance in this example obviously deteriorates, which is in accordance with the previous eigenvalue distribution analysis. However, dynamics of the inter-area oscillation are also mildly improved in comparison to those in the open-loop state.

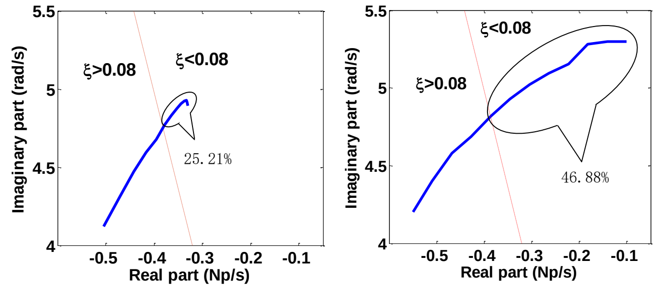

Fig. 5. Distribution of closed-loop inter-area mode in the complex plane (left plot: proposed control design; right plot: robust design)

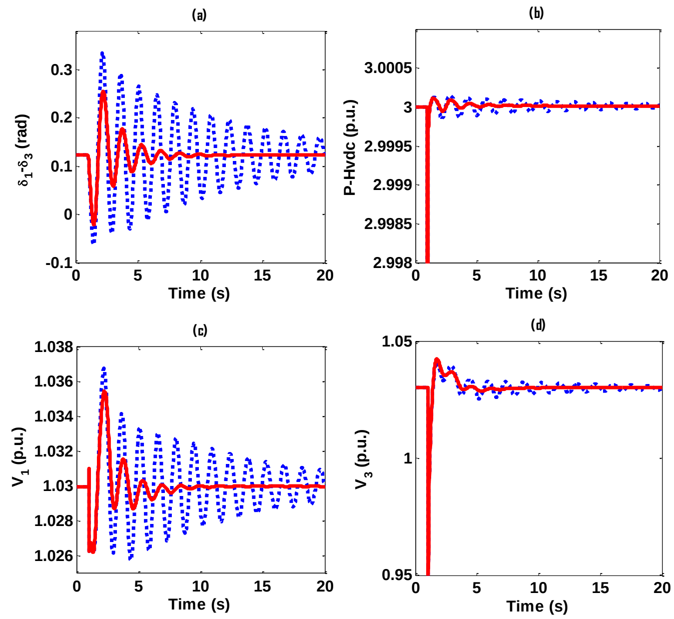

Fig. 6. System dynamics in normal condition with WF's power output being the EV (solid line: closed-loop; dot line: open-loop)

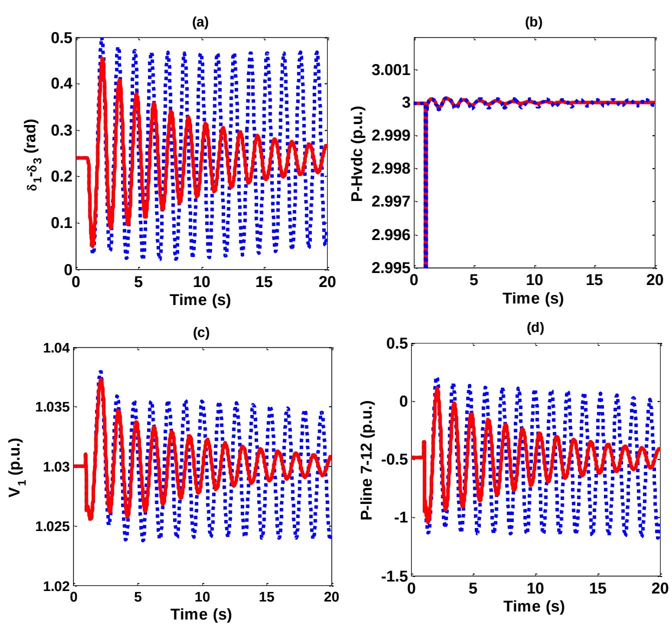

Fig. 7. System dynamics in emergent condition 5 with WF's power output being 100 MW (solid line: closed-loop; dot line: open-loop)

B. New York and New England Interconnected Power System

1) System Description and Settings for Control Design

The classic New York and New England interconnected power system is used with proper modifications to demonstrate the proposed control design (Fig. 8). Three WFs are attached to Bus-70, -71 and -72 via short transmission lines. WF1 and WF3 are aggregately represented by DFIG-based WTs, respectively, and the simulated DFIGs employ the same electromechanical model structure and per-unit parameters [31] as those used in the previous test system. Moreover, a fixed-speed induction generator (FSIG) based WT is used to stand for WF2. The first-order dynamical model (only rotor dynamics are considered) is employed for the FSIG, and the relevant parameters are given in Appendix. A shunt capacitor is also connected to Bus-71 to support the terminal voltage of WF2. WF1, WF2 and WF3 have the installed capacities of 3534 MW (WF_1), 882 MW (WF_2) and 1580 MW (WF_3). Besides, the active loads of Bus-18, -42 and -41 are increased by 1767 MW, 440 MW and 790 MW, respectively. So, the peak penetration level of wind power in the system is around 30%.

A scenario set with 20000 scenarios simulating the actual WPG scenarios of the three WFs in practice is generated by simple random sampling (SRS) based on the marginal CDFs of wind speeds and the WTs' power conversion curves (later, these actual scenarios are used as the comparison benchmark for the proposed control design). It should be pointed out here that calculating FSIG's power conversion is not as simple as (14); the FSIG model should be included in the load flow calculation in order to map the wind speed to the power output of the FSIG. So, the EVs of the three WFs' power outputs are 1770 MW, 440 MW and 790 MW. In these scenarios, as the WFs' steady-state power outputs deviate from their EVs, G_{16}, G_{15} and G_{14} are assigned to be the corresponding synchronous units to compensate the deviations of WF_1, WF_2 and WF_3, respectively. However, it is hypothesized that these synchronous generators have output constraints associated with their capacities or operating conditions so that they cannot entirely accommodate uncertainties of output of the WFs. For example, G_{16} is supposed to be capable of providing adjustable power up to 70% of the maximum or minimum power output deviation (equal to maximum or minimum power output minus the EV) of WF_1 while such data is 55% for G_{15} (to compensate WF_2) and 65% for G_{14} (to compensate WF_3). If the actual power output deviations of the WFs are beyond the adjustment capabilities of the three synchronous units, the residual uncompensated part is balanced by G_{13}. With this dispatching strategy, the steady-state power outputs of G_{13}, G_{14}, G_{15} and G_{16} (deviations with respect to their nominal values) can be expressed as the functions of the WFs' power outputs, as follows:

$$\Delta p_{\mathrm{G16}} = \begin{cases} p_{\mathrm{w1}} - \bar{\mathrm{p}}_{\mathrm{w1}} & 0.7\Delta \mathrm{p}_{\mathrm{w1}}^{\min} \le p_{\mathrm{w1}} - \bar{\mathrm{p}}_{\mathrm{w1}} \le 0.7\Delta \mathrm{p}_{\mathrm{w1}}^{\max} \\ 0.7\Delta \mathrm{p}_{\mathrm{w1}}^{\max} & p_{\mathrm{w1}} - \bar{\mathrm{p}}_{\mathrm{w1}} > 0.7\Delta \mathrm{p}_{\mathrm{w1}}^{\max} \\ 0.7\Delta \mathrm{p}_{\mathrm{w1}}^{\min} & p_{\mathrm{w1}} - \bar{\mathrm{p}}_{\mathrm{w1}} < 0.7\Delta \mathrm{p}_{\mathrm{w1}}^{\min} \end{cases} \tag{15}$$

$$\Delta p_{\mathrm{G15}} = \begin{cases} p_{\mathrm{w2}} - \bar{\mathrm{p}}_{\mathrm{w2}} & 0.55\Delta \mathrm{p}_{\mathrm{w2}}^{\min} \le p_{\mathrm{w2}} - \bar{\mathrm{p}}_{\mathrm{w2}} \le 0.55\Delta \mathrm{p}_{\mathrm{w2}}^{\max} \\ 0.55\Delta \mathrm{p}_{\mathrm{w2}}^{\max} & p_{\mathrm{w2}} - \bar{\mathrm{p}}_{\mathrm{w2}} > 0.55\Delta \mathrm{p}_{\mathrm{w2}}^{\max} \\ 0.55\Delta \mathrm{p}_{\mathrm{w2}}^{\min} & p_{\mathrm{w2}} - \bar{\mathrm{p}}_{\mathrm{w2}} < 0.55\Delta \mathrm{p}_{\mathrm{w2}}^{\min} \end{cases} \tag{16}$$

$$\Delta p_{\mathrm{G14}} = \begin{cases} p_{\mathrm{w3}} - \bar{\mathrm{p}}_{\mathrm{w3}} & 0.65\Delta \mathrm{p}_{\mathrm{w3}}^{\min} \le p_{\mathrm{w3}} - \bar{\mathrm{p}}_{\mathrm{w3}} \le 0.65\Delta \mathrm{p}_{\mathrm{w3}}^{\max} \\ 0.65\Delta \mathrm{p}_{\mathrm{w3}}^{\max} & p_{\mathrm{w3}} - \bar{\mathrm{p}}_{\mathrm{w3}} > 0.65\Delta \mathrm{p}_{\mathrm{w3}}^{\max} \\ 0.65\Delta \mathrm{p}_{\mathrm{w3}}^{\min} & p_{\mathrm{w3}} - \bar{\mathrm{p}}_{\mathrm{w3}} < 0.65\Delta \mathrm{p}_{\mathrm{w3}}^{\min} \end{cases} \tag{17}$$

$$\begin{aligned} &\Delta p_{\mathrm{G13}} + \Delta p_{\mathrm{G14}} + \Delta p_{\mathrm{G15}} + \Delta p_{\mathrm{G16}} = \\ &\quad p_{\mathrm{w1}} - \bar{\mathrm{p}}_{\mathrm{w1}} + p_{\mathrm{w2}} - \bar{\mathrm{p}}_{\mathrm{w2}} + p_{\mathrm{w3}} - \bar{\mathrm{p}}_{\mathrm{w3}} \end{aligned} \tag{18}$$

where Δp_{G} is the power output deviation of the synchronous generator; $\bar{\mathrm{p}}_{\mathrm{w}}$ is the EV of the WF's power output; $\Delta \mathrm{p}_{\mathrm{w}}^{\max} = \mathrm{p}_{\mathrm{w}}^{\max} - \bar{\mathrm{p}}_{\mathrm{w}}$ and $\Delta \mathrm{p}_{\mathrm{w}}^{\min} = \mathrm{p}_{\mathrm{w}}^{\min} - \bar{\mathrm{p}}_{\mathrm{w}}$ with $\mathrm{p}_{\mathrm{w}}^{\max}$ and $\mathrm{p}_{\mathrm{w}}^{\min}$ representing the maximum and minimum power outputs of the WFs, respectively; the number indexes in the subscript of the above variables are used to distinguish different synchronous generators or WFs. Apparently, Δp_{G13}, Δp_{G14}, Δp_{G15} and Δp_{G16} have the characteristic of saturation and are non-smooth with respect to p_{w1}, p_{w2} and p_{w3}.

The configuration of the system shown in Fig. 8 corresponds to the normal condition. Several emergent conditions which are depicted in Table II are also considered. Here, the normal/emergent conditions 0, 1, 2 and 3 are used for the control design while the emergent conditions 4, 5 and 6 are prepared for the validation. It is noted that in every normal/emergent condition, poor damping persists in two inter-area modes (M_1 and M_2) in the simulated system when the operating point varies due to uncertainty of wind power: M_1 has the frequency of around 2.2 rad/s and it dominates the relative oscillation of synchronous generators in AREA #3, #4 and #5 with respect to those in the rest of the system; M_2 with the frequency of about 4.4 rad/s can be obviously identified in the electromechanical oscillatory dynamics between AREA #1 and #2. Therefore, WPSSs are employed to enhance damping of the inter-area modes. The bus frequencies are used as the control inputs of the WPSSs. So, the analysis procedure based on residues calculations presented in the previous test system indicates that G_9 is the most effective unit to place WPSS for damping M_2 while WPSS equipped for G_{13} has the most obvious impacts on M_1. Moreover, among all the buses, the frequency of Bus-17 is found to be the most effective feedback signal for both the WPSSs for damping control; the latency of delivering this signal to G_9 and G_{13} is assumed to be 100 ms and zero, respectively. In addition, $\bar{\xi}_1^{(m)}$ and $\bar{\xi}_2^{(m)}$ are selected to be 0.15 and 0.10, respectively; $\mathrm{WC}_1^{(m)}$ and $\mathrm{WC}_2^{(m)}$ are set to be 20% and 10%, respectively, for all the normal and emergent conditions.

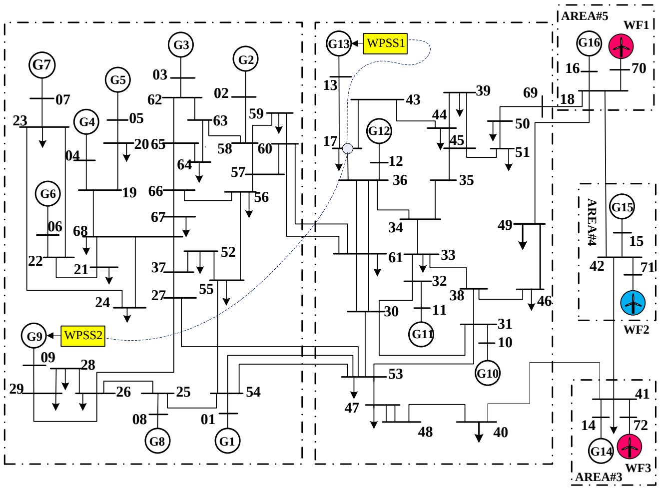

Fig. 8. New York and New England interconnected power system

TABLE II
INDEX $prob^{(m)}$ IN NORMAL/EMERGENT CONDITIONS OF NEW YORK AND NEW ENGLAND INTERCONNECTED SYSTEM

No.	Contingency	Exact	Appr.	Robust
0	Nominal	0.9110	0.8994	0.8408
1	Line 27-53 outage	0.8341	0.8222	0.5674
2	Line 49-18 outage	0.7054	0.6868	0.4468
3	G_{10} outage	0.6137	0.6234	0.5220
4	G_1 outage	0.7202	0.7112	0.4808
5	G_6 outage	0.6756	0.6880	0.5962
6	Line 40-14 outage	0.6310	0.6202	0.4726

According to the procedure presented in Section IV-A, a total of 500 (N_t=500) scenarios are produced for the proposed control design. It is known that the marginal CDFs of the WFs' power outputs and coefficients of correlations among them derived from these simulated scenarios are close to those obtained from the actual scenarios (with the number of 20000). Moreover, for each normal/emergent condition, the open-loop nonlinear system models having the orders larger than 200 (the model orders are different in some emergent conditions) are linearized in all the simulated WPG scenarios and uniformly reduced to the 20th order models by the Schur balanced truncation method. One reduced model is selected to conduct the impulse response test, and Fig. 9 compares the result with that obtained based on its original full state-space model. It is found that curves derived from the two models are almost overlapped. Therefore, it can be concluded that both M_1 and M_2 are exactly kept in this order-reduced system which is accurate enough to represent the input-output dynamics of the original system. Indeed, the same conclusion is obtained for all the other reduced models. During the search process, N_p and N_e are set to be 60 and 5, respectively. Moreover, the optimization weights ($W^{(0)}$, $W^{(1)}$, $W^{(2)}$ and $W^{(3)}$) for the normal and emergent conditions are set to be 1.0, 0.5, 0.5 and 0.5, respectively.

2) Search Efficiency and Capability of Customized DE

It takes around 1.25 hours to accomplish linearization and the subsequent reduction of the open-loop power system models over all the reduced WPG scenarios in the normal and emergent conditions. However, this time cost of preprocessing the models indeed contributes to the benefit that calculating the objective function with the reduced WPG scenarios and the reduced models averagely costs just 1.03 s (this time consumption is 80 s if neither model reduction nor WPG scenario reduction is conducted).

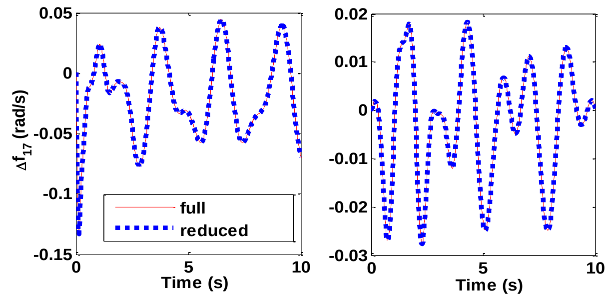

Fig. 9. Impulse response of full and reduced models (left plot: input from WPSS1; right plot: input from WPSS2)

As conducted in the previous test case, average performance of the proposed customized DE is further justified by solving the optimization problem in this test system which is obviously much more complicated. Specifically, it is run 20 times to solve the maximization (6)-(10) and each run evolves 700 generations. It is found that most runs take less than 580 generations to reach their respective maxima which is very close to the maximum objective function (1.9656) derived over all the runs. Furthermore, running the standard DE to solve the problem is also conducted for direct comparison. Since this run is fairly time consuming, it is only conducted once. The standard DE costs 655 generations to converge to the maxima of 1.9656. Only from this simple comparison, it is believed that the average search quality (in terms of the obtained maxima and the necessary generations to reach this maxima) of the customized DE is never inferior to that of the standard DE. Therefore, as concluded at the previous test system, it has been proved again that the customized DE can efficiently solve the formulated optimization problem and the computational time is much lower than that of directly using the standard DE.

C. Performance of Optimal WPSSs

The optimal parameters vector that results in the maximum objective function over all the search runs in the previous subsection is provided in Appendix. So, the actual scenarios are used to demonstrate the control effects of the WPSSs with the optimal parameters.

Firstly, the accuracy of derived result should be examined. Thus, the index $Prob^{(m)}$ is calculated for each normal/emergent condition. Again, the value of $Prob^{(m)}$ which is computed based on the real WPG scenarios and the full system models is used as the benchmark. The approximate $Prob^{(m)}$ is calculated by using the reduced WPG scenarios and the reduced models, and is also compared with the benchmark in Table II. Clearly, the favorable approximation effects in all the normal and emergent conditions once again prove that the proposed method to reduce the computational burden during the optimization is accurate and effective.

According to Table II, compared to the open-loop situations, the probabilities of the event that M_1 and M_2 simultaneously have the required damping ratios are enhanced by the tuned WPSSs in the normal/emergent conditions which are directly included in the optimization, but also in the emergent conditions which are used just for validation. This probability promotion is especially apparent in the normal condition because of the obviously bias optimization weights setting. The proposed control design is compared with the common robust design used in the previous test case in terms of their derived $Prob^{(m)}$ in the normal/emergent conditions. The clear superiority of the proposed control design over the robust design can be observed in Table II, especially in the emergent conditions. For example, Fig. 10 shows the joint distribution of damping ratios of M_1 and M_2 in the emergent condition 3, which is a strong evidence to support the above conclusion.

It is necessary to further verify the probabilistic robustness of the derived WPSSs by time-domain simulations under multiple operating points. Although a number of test scenarios have been applied, only three of them are described here due to the space limitation: (a) the system is in the normal condition and the WFs' power outputs are their respective EVs. The fault is a 100 ms instantaneous three-phase fault occurring at Bus-42; (b) G_1 is outage and its power supply duty is taken by G_9. The WFs' power outputs and the fault are the same as those in the previous test scenario; (c) the power outputs of WF1, WF2 and WF3 are 100 MW, 100 MW and 100 MW, respectively; the system is in the normal condition and subjected to a permanent three-phase fault happening at line 49-18; the fault is cleared by tripping the faulty line and no re-closure is conducted. Parts of the relative load angles of the synchronous generators are depicted in Fig. 11. It is seen that besides the excellent performance in the normal condition, the WPSSs can also correctly behave to provide damping to the inter-area oscillations as the system is in the emergent conditions (heavily loaded generator or tie-line is lost).

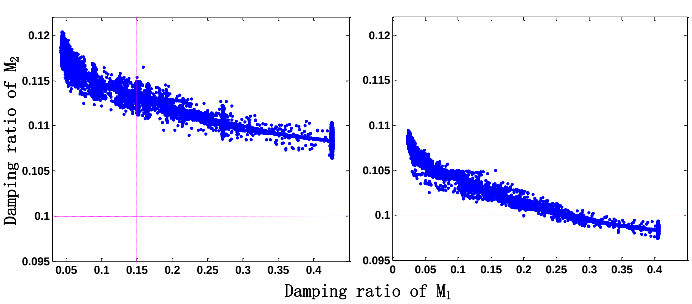

Fig. 10. Joint distribution of damping ratios of M_1 and M_2 (left plot: controllers tuned by proposed method; right plot: controllers tuned by robust design)

VII. Conclusion

The operating points of power systems with huge amounts of wind power integration vary stochastically over quite a wide range. Thus, the conventional control designs aiming to improve the damping of inter-area oscillations of a system normally fail to deliver the required performance in the sense of probabilistic stability since they overlook the system's stochastic nature. In this paper, a systematic approach has been proposed to tune the WPSSs with the traditional phase lead-lag structure to achieve the probabilistic robustness for damping the inter-area oscillations of power systems incorporating wind power. Moreover, multiple contingencies are directly taken into account during the control design. In other words, the tuned WPSSs can maximize the proportion of the WPG scenarios where all inter-area modes simultaneously have the required damping ratios, and also constraint their adverse impacts properly over all the WPG scenarios in the normal and emergent conditions. Moreover, employment of the advanced scenario generation and model reduction techniques to lower the computational intensity of the probability evaluations and proposal of a customized DE to solve the optimization problem can ensure the accuracy and efficiency of the proposed tuning method. Simulations on the modified two-area system and New York and New England interconnected system have demonstrated that the WPSSs tuned by the proposed method are very superior to those tuned by the conventional method.

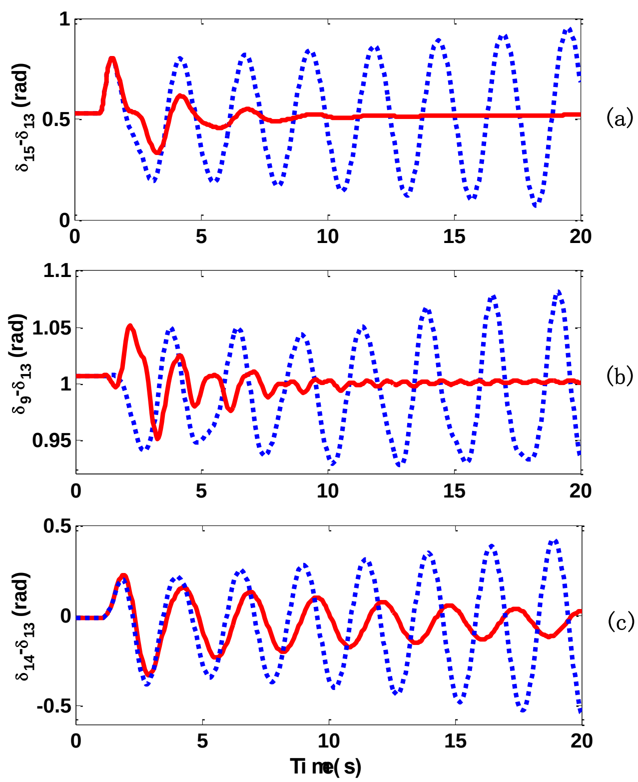

Fig. 11. Relative load angle of synchronous generators under different test scenarios (solid line: closed-loop; dot line: open-loop).

Appendix

A. Deduction of State Matrix of Closed-Loop System

The full linear model (state matrix **A**, input matrix **B**, and output matrix **C**) of the open-loop power system is acquired by using PSAT (version 2.1.4) [30]. Indeed, one important feature of PSAT is separately analytical linearization of system components such as synchronous generators and power network. Moreover, a smart mechanism is used by PSAT to systematically assemble these linearized components and thus conveniently produce the linearized differential and algebraic equations. Therefore, the linear state-space model is synthesized by eliminating the algebraic variables in the differential equations. Actually, PSAT packages the analytical calculation of linearized model in the function 'fm_abcd' and stores the result in the global structure 'LA'.

Based on symbols introduced in Section II, the state-space equations of the open-loop power system, the approximated time-delay (by Pade formula) and the WPSSs can be represented by (19), (20) and (21), respectively:

$$\begin{cases} \dot{\boldsymbol{X}}_{\mathrm{o}} = \mathbf{A}_{\mathrm{o}}^{(i,m)}\boldsymbol{X}_{\mathrm{o}} + \mathbf{B}_{\mathrm{o}}^{(i,m)}\boldsymbol{u}_{\mathrm{c}} \\ \boldsymbol{Y}_{\mathrm{o}} = \mathbf{C}_{\mathrm{o}}^{(i,m)}\boldsymbol{X}_{\mathrm{o}} \end{cases} \tag{19}$$

$$\begin{cases} \dot{\boldsymbol{X}}_{\tau} = \mathbf{A}_{\tau}\boldsymbol{X}_{\tau} + \mathbf{B}_{\tau}\boldsymbol{Y}_{\mathrm{o}} \\ \boldsymbol{Y}_{\mathrm{m}} = \mathbf{B}_{\tau}\boldsymbol{X}_{\tau} + \mathbf{D}_{\tau}\boldsymbol{Y}_{\mathrm{o}} \end{cases} \tag{20}$$

$$\begin{cases} \dot{\boldsymbol{X}}_{\mathrm{c}} = \mathbf{A}_{\mathrm{c}}\boldsymbol{X}_{\mathrm{c}} + \mathbf{B}_{\mathrm{c}}\boldsymbol{Y}_{\mathrm{m}} \\ \boldsymbol{u}_{\mathrm{c}} = \mathbf{C}_{\mathrm{c}}\boldsymbol{X}_{\mathrm{c}} + \mathbf{D}_{\mathrm{c}}\boldsymbol{Y}_{\mathrm{m}} \end{cases} \tag{21}$$

where $\boldsymbol{X}_{\mathrm{o}}$, $\boldsymbol{X}_{\tau}$ and $\boldsymbol{X}_{\mathrm{c}}$ are the state variables vectors of the open-loop system, the approximated time-delay and the WPSSs, respectively; $\boldsymbol{u}_{\mathrm{c}}$ is the control input of the open-loop system, i.e., the supplementary voltage reference of exciter; $\boldsymbol{Y}_{\mathrm{o}}$ is the output of the open-loop system, i.e., the bus frequency; $\boldsymbol{Y}_{\mathrm{o}}$ is delayed by the wide-area communication system and becomes $\boldsymbol{Y}_{\mathrm{m}}$ which is the signal received by the WPSSs; thus, $\boldsymbol{Y}_{\mathrm{m}}$ is used as the input of the WPSSs which produce the output $\boldsymbol{u}_{\mathrm{c}}$ to control the power system. The first step to synthesize the closed-loop state matrix is to combine (19) and (20). So, the state-space equation of the combined system is derived by merging $\boldsymbol{X}_{\mathrm{o}}$ and $\boldsymbol{X}_{\tau}$ as one state variables vector and using $\boldsymbol{Y}_{\mathrm{m}}$ as the output of the merged system to eliminate $\boldsymbol{Y}_{\mathrm{o}}$:

$$\begin{cases} \begin{bmatrix} \dot{\boldsymbol{X}}_{\mathrm{o}} \\ \dot{\boldsymbol{X}}_{\tau} \end{bmatrix} = \begin{bmatrix} \mathbf{A}_{\mathrm{o}}^{(i,m)} & \mathbf{0} \\ \mathbf{B}_{\tau}\mathbf{C}_{\mathrm{o}}^{(i,m)} & \mathbf{A}_{\tau} \end{bmatrix} \begin{bmatrix} \boldsymbol{X}_{\mathrm{o}} \\ \boldsymbol{X}_{\tau} \end{bmatrix} + \begin{bmatrix} \mathbf{B}_{\mathrm{o}}^{(i,m)} \\ \mathbf{0} \end{bmatrix} \boldsymbol{u}_{\mathrm{c}} \\ \boldsymbol{Y}_{\mathrm{m}} = \begin{bmatrix} \mathbf{D}_{\tau}\mathbf{C}_{\mathrm{o}}^{(i,m)} & \mathbf{B}_{\tau} \end{bmatrix} \begin{bmatrix} \boldsymbol{X}_{\mathrm{o}} \\ \boldsymbol{X}_{\tau} \end{bmatrix} \end{cases} \tag{22}$$

Then, the operation is to merge (21) and (22) by mutual input-output combination to eliminate $\boldsymbol{u}_{\mathrm{c}}$ and $\boldsymbol{Y}_{\mathrm{m}}$, finally yielding the close-loop state matrix as shown in Section II.

B. Optimal Parameters of the WPSSs

Here, System 1 denotes the two-area system and the New York and New England interconnected system is System 2.

TABLE III
OPTIMAL PARAMETERS OF WPSSs

	System 1	System 2
K_1	12.6334	23.3009
T_{w1}	14.9600	8.5654
T_{b1}	1.2014	1.2469
T_{u1}	0.4803	0.7268
K_2	17.5780	18.5643
T_{w2}	14.5000	9.5000
T_{b2}	0.9776	0.5924
T_{u2}	0.4235	0.1141

C. Model Parameters

DFIG and FSIG Parameters (on Base of Machine Rating, 700 MVA): R_s = 0.00488, R_r = 0.00549, X_s = 0.09241, X_r = 0.09955, X_m = 3.95279, H = 3.5 s. Operating slip range of FSIG: [-0.016, 0]. WT radius: 35 m. Gear box ratio: 74. Power coefficient of WT: C_p=0.73(151/λ-13.654)exp(-18.4/λ+0.0552).

REFERENCES

[1] H. Huang, C. Y. Chung, K. W. Chan, and H. Chen, "Quasi-Monte Carlo based probabilistic small signal stability analysis for power systems with plug-in electric vehicle and wind power integration," *IEEE Trans. Power Syst*., vol. 28, no. 3, pp. 3335-3343, Aug. 2013.

[2] D. Gautam, V. Vittal, and T. Harbour, "Impact of increased penetration of DFIG-based wind turbine generators on transient and small-signal stability of power systems," *IEEE Trans. Power Syst*., vol. 24, no. 3, pp. 1426-1434, Aug. 2009.

[3] Y. Sun, L. Wang, G. Li, and J. Lin, "A review on analysis and control of small signal stability of power systems with large scale integration of wind power," presented at the 7th Int. Conf. Power System Technology, Hangzhou, China, Oct. 24-28, 2010.

[4] G. Tsourakis, B. M. Nomikos, and C. D. Vournas, "Contribution of doubly fed wind generators to oscillation damping," *IEEE Trans. Energy Convers*., vol. 24, no. 3, pp. 783-791, Jul. 2009.

[5] F. M. Hughes, O. Anaya-Lara, N. Jenkins, and G. Strbac, "A power system stabilizer for DFIG-based wind generation," *IEEE Trans. Power Syst*., vol. 21, no. 2, pp. 763-772, May. 2006.

[6] Z. Miao, L. Fan, D. Osborn, and S. Yuvarajan, "Control of DFIG-based wind generation to improve interarea oscillation damping," *IEEE Trans. Energy Convers*., vol. 24, no. 2, pp. 415-422, Jun. 2009.

[7] L. Fan, H. Yin, and Z. Miao, "On active/reactive power modulation of DFIG-based wind generation for interarea oscillation damping," *IEEE Trans. Energy Convers*., vol. 26, no. 2, pp. 513-521, Jun. 2011.

[8] A. E. Leon and J. A. Solsona, "Power oscillation damping improvement by adding multiple wind farms to wide-area coordinating controls," *IEEE Trans. Power Syst*., vol. 29, no. 3, pp. 1356-1364, May. 2014.

[9] N. R. Chaudhuri and B. Chaudhuri, "Considerations toward coordinated control of DFIG-based wind farms," *IEEE Trans. Power Del*., vol. 28, no. 3, pp. 1263-1270, Jul. 2013.

[10] D. P. Ke, C. Y. Chung, and Y. Xue, "Controller design for DFIG-based wind power generation to damp interarea oscillation," presented at the 5th Int. Conf. critical infrastructure (CRIS), Beijing, China, Sep. 20-22, 2010.

[11] M. Mokhtari and F. Aminifar, "Toward wide-area oscillation control through doubly-fed induction generator wind farms," *IEEE Trans. Power Syst*., vol. 29, no. 6, pp. 2985-2992, Nov. 2014.

[12] D. F. Gayme and A. Chakrabortty, "A spatio-temporal framework for spectral analysis and control of interarea oscillations in wind-integrated power systems," *IEEE Trans. Control Syst., Technol*., vol. 22, no. 4, pp. 1658-1665, Jul. 2014.

[13] T. Knuppel, J. N. Nielsen, K. H. Jensen, A. Dixon, and J. Ostergaard, "Power oscillation damping capabilities of wind power plant with full converter wind turbines considering its distributed and modular characteristics," *IET Renew. Power Gener*., vol. 7, no. 5, pp. 431-442, 2013.

[14] G. Xu, L. Xu, and J. Morrow, "Power oscillation damping using wind turbines with energy storage systems," *IET Renew. Power Gener*., vol. 7, no. 5, pp. 449-457, 2013.

[15] Y. Liu, J. R. Gracia, T. J. King, and Y. Liu, "Frequency regulation and oscillation damping contributions of variable-speed wind generators in the U. S. Eastern interconnection (EI)," *IEEE Trans. Sustain. Energy*, vol. 6, no. 3, pp. 951-958, Jul. 2015.

[16] S. Golshannavaz, F. Aminifar, and D. Nazarpour, "Application of UPFC to enhancing oscillatory response of series-compensated wind farm integrations," *IEEE Trans. Smart Grid*, vol. 5, no. 4, pp. 1961-1968, Jul. 2014.

[17] A. E. Leon, J. M. Mauricio, A. Gomez-Exposito, and J. A. Solsona, "Hierarchical wide-area control of power systems including wind farms and FACTS for short-term frequency regulation," *IEEE Trans. Power Syst*., vol. 27, no. 4, pp. 2084-2092, Nov. 2012.

[18] J. Morato, T. Knuppel, and J. Ostergaard, "Residue-based evaluation of the use of wind power plants with full converter wind turbines for power oscillation damping control," *IEEE Trans. Sustain. Energy*, vol. 5, no. 1, pp. 82-89, Jan. 2014.

[19] S. Chandra, D. F. Gayme, and A. Chakrabortty, "Coordinating wind farms and battery management systems for inter-area oscillation damping: a frequency domain approach," *IEEE Trans. Power Syst*., vol. 29, no. 3, pp. 1454-1462, May 2014.

[20] S. Q. Bu, W. Du, H. F. Wang, Z. Chen, L. Y. Xiao, and H. F. Li, "Probabilistic analysis of small-signal stability of large-scale power systems as affected by penetration of wind generation," *IEEE Trans*. *Power Syst*., vol. 27, no. 2, pp. 762-770, May 2012.
[21] C. A. Juarez, J. L. Rueda, I. Erlich, and D. G. Colome, "Probabilistic approach-based wide-area damping controller for small-signal stability enhancement of wind-thermal power systems," presented at the IEEE PES general meeting, Detroit, USA, Jul. 24-29, 2011.
[22] T. Surinkaew and I. Ngamroo, "Coordinated robust control of DFIG wind turbine and PSS for stabilization of power oscillations considering system uncertainties," *IEEE Trans*. *Sustain*. *Energy*, vol. 5, no. 3, pp. 823-833, Jul. 2014.
[23] H. Huang and C. Y. Chung, "Coordinated damping control design for DFIG-based wind generation considering power output variation," *IEEE Trans. Power Syst*., vol. 27, no. 4, pp. 1916-1925, Nov. 2012.
[24] R. Preece and J. V. Milanovic, "Tuning of a damping controller for multiterminal VSC-HVDC grids using the probabilistic collocation method," *IEEE Trans. Power Del*., vol. 29, no. 1, pp. 318-326, Feb. 2014.
[25] D. P. Ke and C. Y. Chung, "An inter-area mode oriented pole-shifting method with coordination of control efforts for robust tuning of power oscillation damping controllers," *IEEE Trans*. *Power Syst*., vol. 27, no. 3, pp. 1422-1432, Aug. 2012.
[26] P. Kundur, Power System Stability and Control. New York, NY, USA: McGraw-Hill, 1994.
[27] H. Yu, C. Y. Chung, K. P. Wong, and J. H. Zhang, "Probabilistic load flow evaluation with hybrid Latin Hypercube Sampling and Cholesky decomposition," *IEEE Trans*. *Power Syst*., vol. 24, no. 2, pp. 661-667, May 2009.
[28] F. D. Freitas, J. Rommes, and N. Martins, "Gramian-based reduction method applied to large sparse power system descriptor models," *IEEE Trans. Power Syst*., vol. 23, no. 3, pp. 1258-1270, Aug. 2008.
[29] K. Price, R. M. Storn, and J. A. Lampinen, *Differential Evolution: A Practical Approach to Global Optimization*, Springer, 2005.
[30] F. Milano, Power System Analysis Toolbox: http://www.uclm.es/area/gsee/Web/Federico/psat.htm.
[31] O. Anaya-Lara, N. Jenkins, J. Ekanayake, P. Cartwright, and M. Hughes, *Wind Energy Generation—Modelling and Control*, Wiley, 2009.

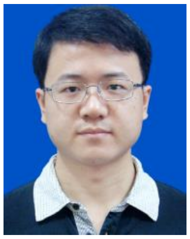

Deping Ke received the B.S degree in Electrical Engineering in 2005 from Huazhong University of Science and Technology, Wuhan, China, and the Ph.D. degree in Electrical Engineering from The Hong Kong Polytechnic University in 2012. Currently, he is a lecturer with the School of Electrical Engineering, Wuhan University, China. His research interests are in power system dynamics and control, and economic operation of power systems.

C. Y. Chung (M'01–SM'07-F'16) received the Ph.D. degree in electrical engineering from The Hong Kong Polytechnic University in 1999. He is currently a Professor and the SaskPower Chair in Power Systems Engineering in the Department of Electrical and Computer Engineering at the University of Saskatchewan, Saskatoon, SK, Canada. His research interests include power system stability/control, planning and operation, computational intelligence applications, power markets, and electric vehicle charging. Dr. Chung is an Editor of the IEEE TRANSACTIONS ON SUSTAINABLE ENERGY and an Editorial Board Member of IET GENERATION, TRANSMISSION & DISTRIBUTION. He is also a Member-at-Large (Smart Grid) of IEEE PES Governing Board and the IEEE PES Region 10 North Chapter Representative.